Experimental study of stability, quench propagation and detection methods on 15 kA sub-scale HTS fusion conductors in SULTAN

N. Bykovskiy[1], H. Bajas[1], O. Dicuonzo[2], P. Bruzzone[1], and K. Sedlak[1]

[1] École Polytechnique Fédérale de Lausanne (EPFL), Swiss Plasma Center (SPC), CH-5232 Villigen PSI, Switzerland
[2] former at École Polytechnique Fédérale de Lausanne (EPFL), Swiss Plasma Center (SPC), CH-5232 Villigen PSI, Switzerland

Corresponding author: nikolay.bykovskiy@psi.ch

Abstract. High-temperature superconductors (HTS) enable exclusive operating conditions for fusion magnets, boosting their performance up to 20 T generated magnetic fields, in the temperature range from 4 K to 20 K. One of the main technological issues of the HTS conductors is focused on their protection in the case of a thermal runaway (quench). In spite of extremely high thermal stability of HTS materials, quench is still possible due to local defects along the conductor length or insufficient cooling. In such cases, the high stability results in slow propagation of a resistive zone. Thereby, risky hot-spot temperature (>200 K) can be reached, if applying conventional quench detection methods at the voltage threshold of 0.1 – 0.5 V, typical for fusion magnets. Aiming at experimental study of the phenomenon, a series of sub-scale 15 kA 3.6 m long conductors based on stack of tapes soldered in copper profiles are manufactured at Swiss Plasma Center, including twisted ReBCO and BISCCO triplets, non-twisted and solder-filled ReBCO triplets, as well as indirectly cooled non-twisted ReBCO single strand. Applying either increasing helium inlet temperature, overcurrent operation or energy deposited by embedded cartridge heaters, critical values of the electric field and temperature are evaluated for a given operating current (up to 15 kA) and background magnetic field (up to 10.9 T). Once quench is actually triggered, the quench propagation is studied by distributed voltage taps and temperature sensors able to monitor the external temperature of the jacket and internal one of the conductor (helium or copper). Thanks to the recent upgrade of the SULTAN test facility, quench propagation in the conductors is measured up to the total voltage of 2 V and peak temperature of 320 K. Furthermore, novel quench detection methods based on superconducting insulated wires and fiber optics are also instrumented and studied. Summary of the test samples, their instrumentation and corresponding test results is presented in this work.

Keywords: HTS fusion conductors, thermal stability, quench propagation, quench detection

1. Introduction

Recent advances in the technology of high-temperature superconductors (HTS), such as increased critical current density and higher production yield, turn finally the possibility for HTS-based fusion magnets into a practical matter. Among a variety of the high-current HTS conductor designs proposed for fusion magnets, the relevant demonstrations have already been performed on the certain twisted stacked-tape concepts ([1], [2]), whereas the other twisted stacked-tape variants ([3], [4], [5], [6]) as well as the CORC conductors [7] are yet to be tested. Simplified concepts based on the straight stack of tapes are also considered for the coil windings operated in stationary mode ([8], [9], [10]).

The need of HTS for fusion magnets is essentially motivated by increasing the generated magnetic fields, which allows improving the overall performance of the fusion machines [11]. In the case of the EU-DEMO magnet system, the innermost layers of the central solenoid (CS) made of HTS conductors can increase the baseline operation at 12 T in coils up to 19 T, thus strongly increasing the available magnetic flux [12]. As a result, by achieving longer plasma burn time, an effective power of the demonstration reactor can be increased by some 10-20%.

The feasibility study on HTS conductors for DEMO CS is aiming currently at the optimal conductor layout resilient to strong cyclic electromagnetic loading (up to 1100 kN/m), tolerant to potential crack formation in the steel jacket due to fatigue issues and also featuring sufficiently low AC losses caused by the pulsed coil operation (up to ~1 T/s) [13]. Although it must ensure the nominal operation of the CS modules, potential failure modes such as loss of cooling or presence of defects along the conductor length may result in an uncontrolled thermal runaway ('quench'), despite of high stability of the HTS materials. Hence, quench detection and protection aspects have to be also addressed.

A variety of the quench detection methods is being considered for HTS. Using the voltage taps is the most common electrical method providing robust and repairable instrumentation. However, in order to exclude large inductive components present during the operation of fusion magnets, voltage taps need to be co-wound together with the main conductor [14], thus losing the reparability feature. Furthermore, compared to low temperature superconductors (LTS), a much slower propagation of resistive zone in HTS during a quench raises concerns whether the co-wound voltage taps are sensitive enough for a timely detection. Enhanced sensitivity of the co-wound voltage taps can be achieved by using superconducting wires ([15], [16], [17], [18]). By establishing a good thermal contact with the main conductor, the voltage response can be strongly increased due to a much higher off-state resistance of the superconducting quench detection (SQD) wires compared to the main conductor. In that regard, the SQD wires can be considered as an exotic distributed temperature sensors, which can only indicate whether the operating temperature exceeds corresponding critical temperature at a given magnetic field somewhere along the wire length. To further enhance the noise cancellation performance, the SQD wires can be integrated as a twisted pair, which is electrically insulated from the main conductor along the entire length.

An overview on the non-voltage detection techniques based on magnetic, optical and acoustic phenomena can be found in [19]. Most of them have rather complex response caused, for example, by integral sensing of Hall probes, pickup coils and acoustic sensors or dependence on mechanical strain of optical fibers. It requires thorough interpretation of the detection signal in order to achieve sufficient sensitivity and to avoid false positives at the same time. Detecting a quench during a magnet charge or a fast transient operation, corresponding to the highest chance of quenching, is especially challenging by these techniques. Nonetheless, the active development of these techniques is on-going and promising results are reported by various groups (for example, see [20], [21], [22], [23]).

Large fusion magnets are commonly protected by extraction of the stored magnetic energy (E) using an external dump resistor. Negligible amount of the energy is then released in the coil winding itself, but high operating currents (I) and high discharge voltages (V) are required to decrease the discharge time constant $\tau = 2E/(IV)$. The protection criteria is set at peak temperature at the location of hot-spot, typically 150 K on the conductor jacket and ~250 K in the cable. In combination with the time constant order of 10 to 30 s, the criteria usually results in relatively large amount of the stabilizing copper, corresponding to copper current density ~100 A/mm^2.

In contrast, compact fully HTS fusion magnets explore an 'opposite' protection approach using non-insulated coil windings, thus dumping the stored energy into the cold mass. To the authors' knowledge, the method is first proposed for LTS windings in [24] and it became a wide-spread approach once it was also applied for HTS windings [25]. This enables much higher operating current densities and negligible discharge voltages, however such windings are only suitable for a slow operation to prevent large parasitic currents between the turns. Complicated mechanical loadings during a quench and long cooling times to recover the nominal operation should also be addressed. In that regard, an 'intermediate' protection approach based on insulated windings protected by a partial internal energy dump provided by a co-wound heater can be considered as a trade-off. High power required for a sufficient heating of the winding can actually be obtained from the stored magnetic energy by implementing a high current switch in parallel with the co-wound heater and external dump resistor. In this case, the dump resistor can be rated for much lower discharge voltages compared to conventional external energy dump.

Experimental investigations on the quench characteristics of the cable-in-conduit conductors were mostly focused on stability aspects of LTS and qualification of the detection methods (see [26], [27], [28], [29], [30]). For instance, the QUELL experiment in SULTAN was an extensive test campaign that allowed to reveal the dominant regimes of the normal zone propagation, strongly affected by the cooling aspects. It also highlighted the advantages of the embedded co-wound voltage taps and optical fiber detection methods over the hydraulic techniques based on the absolute pressure and mass flow rate of helium [31]. The hot-spot evolution has also been studied experimentally [32], indicating at the importance of a thermal coupling between the cable and jacket.

Quench considerations on HTS fusion conductors were mostly focused on the development of numerical models (see [33], [34], [35]). The case of graded EU DEMO central solenoid was also analysed recently in [36]. Although the predicted quench performance is often found acceptable, the analyses are inevitably prone to certain modelling assumptions such as lumped-element geometry, fixing the thermal coupling parameters, voltage-current transition metrics and quench detection characteristics. In order to perform relevant experiments on HTS fusion conductors, the SULTAN test facility was upgraded by a new test insert allowing a direct drive operation up to 15 kA transport current and 10 V operating voltage [37], complementing its regular low voltage operation up to 100 kA using superconducting transformer. This provides the possibility to maintain the DC currents in the temperature range from 5 K to 300 K using a forced flow helium cooling. The first test results obtained on triplet conductors made of soldered ReBCO stacks are discussed in [38]. As reported in [39], the obtained data allowed to benchmark the 1-D thermal-hydraulic and electrical models and refine the assessment of the quench performance for the EU DEMO central solenoid.

Recently, the two more 'quench experiments' have been performed in SULTAN on sub-size 15 kA conductors made of BISCCO and ReBCO tapes. Apart from the voltage and temperature monitoring, the new conductors are also equipped with the two types of promising quench detection sensors for fusion magnets. The first one is a modification of co-wound voltage taps by using non-stabilized SQD wires embedded in the conductor jacket and operated at relatively low transport current, ~0.1 A. This aims at increased detection sensitivity compared to the conventional technique according to the results presented in [40]. The second one is an optical interferometer containing two plain fibers (i.e. without gratings), one is on the conductor jacket and another is a reference arm, which form a closed optical circuit. The obtained interference pattern converted to electrical signal should serve as a detection trigger [41]. Both methods are of integral-type sensing, not suitable to identify location of the hot-spot and aiming only at '0/1' response for the quench detection.

A summary of the SULTAN quench experiments is provided in this work, starting by an overview of the measured HTS conductors and their instrumentation in the next section. The test results are presented by focusing first on the stability aspects, following by the quench propagation dynamics and detection characteristics of the SQD wires and fiber optics. A simplified method to evaluate the total voltage and hot-spot temperature is formulated and applied in the consideration of the insulated coil windings protected by external energy dump.

2. Overview of the test samples

All the measured conductors are made of soldered stacks of HTS tapes. Following the former full-scale HTS conductor development at SPC [42], the first four of them contain the stacks between the two semi-circular copper profiles forming the round strands of 8.5 mm diameter. Using the three strands, a triplet cable geometry is then constructed. Both the strands and triplets are twisted at the twist-pitch of 400 mm and 1000 mm, except the 'no-twist' conductor where the stack orientation is always perpendicular to the external magnetic field (i.e. the DC SULTAN magnetic field is along the c-axis of the tapes), see Table 1. The triplets are inserted into a stainless steel tube of 8.5 mm wall thickness and eventually crimped to close the insertion tolerance. For the 'filled' conductor, the triplets are filled with $Bi_{57}Sn_{42}Ag_1$ solder inside a U-shape groove of the rectangular steel jacket and the steel lid is then welded on top of it. The strands of the 'BISCCO' conductor have increased slot dimensions, from 3.4 *x* 2.4 mm^2 of the previous conductors up to 4.5 *x* 4.5 mm^2, in order to accommodate the wider and thicker BISCCO tapes.

Table 1. Illustration of the measured conductors and summary of their main properties.

Conductor	Ref	No-twist	Filled	BISCCO	ASTRA
Cross-section	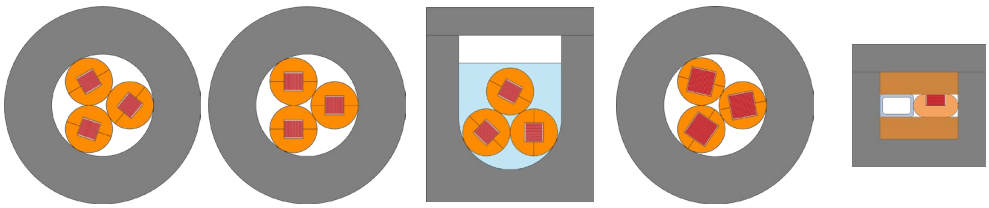				
Features	Twisted strands and triplet	Straight strands and triplet, perpend. field	Twisted strands and triplet, solder filled	Twisted strands and triplet	Straight strand, parallel field, indirect cooling
Superconductor	3.0 mm width *x* 25 tapes *x* 3 stacks			4.2 mm *x* 19 *x* 3	3.3 mm *x* 21 *x* 1
Copper	150 mm^2	150 mm^2	150 mm^2	109 mm^2	144 mm^2
Steel	715 mm^2	715 mm^2	652 mm^2	715 mm^2	360 mm^2

The two more studied conductors are a sub-size version of the so-called 'ASTRA' conductor (Aligned Stacks Transposed in Roebel Arrangement), which is proposed recently for the application in the central solenoid of the EU DEMO magnet [13]. The tape stack is oriented parallel to the external field, thus only one strand is used to achieve the target operation at 15 kA/10.9 T due to higher critical currents. The strand is cooled 'indirectly' through a contact with the top and bottom copper bars delivering the cooling power from the tight cooling channel. Because of that, indium tapes are included in the contact and the conductor components are pre-compressed before the jacket welding in order to decrease thermal resistance of the cooling path. Except the BISCCO conductor, the rest of them are made of ReBCO tapes provided by SST.

The conductors of about 3.6 m length are paired electrically in series and hydraulically in parallel to form a SULTAN sample. The voltage taps are distributed along the length at the distance down to 100 mm in the region located in the high field zone of SULTAN, see Figure 1. The CERNOX temperature sensors are either placed on the conductor jacket or integrated within the cable space. The latter option is done by using Swagelok fittings providing demountable and helium leak-tight instrumentation. In this case, the six sensors are facing the helium flow in each of the triplet conductors, whereas for the ASTRA conductors the six of them ('TH1-6') are touching the strand, the cooling channel and the copper bars.

The conductors are cooled by a forced flow of helium through a dedicated space within the steel jacket, namely the voids between the strands for the Ref, No-Twist and BISCCO conductors and the rectangular space between the solder domain and the top jacket plate for the Filled conductor. Both options correspond

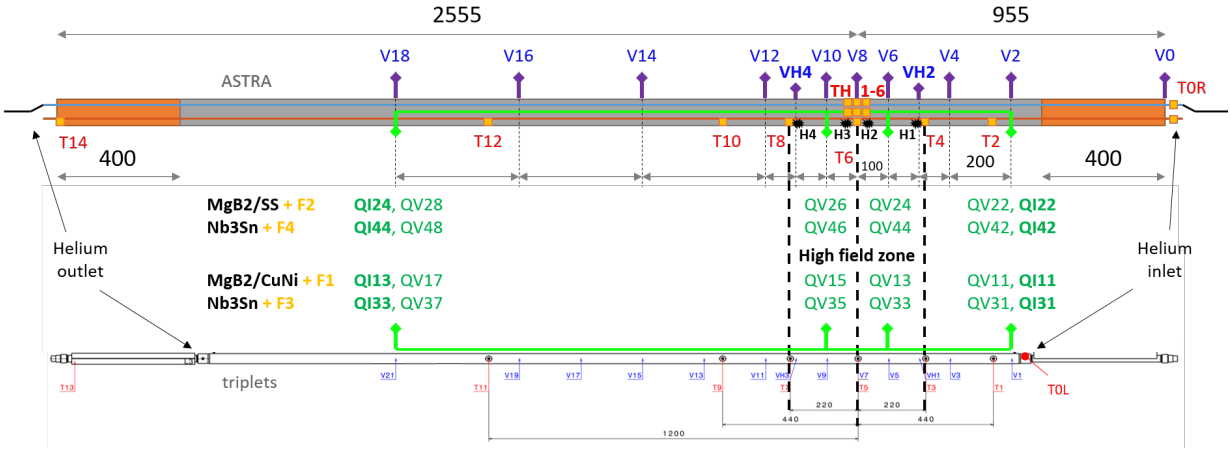

Figure 1. Schematic instrumentation of the SULTAN samples showing positions of the voltage taps ('Vxx') and temperature sensors ('Txx'). The ASTRA and BISCCO conductors include also the SQD wires installed on the jacket surface ('QIxx' for current terminals, 'QVxx' for voltage taps) and optical fibers ('Fx'). Cartridge heaters are embedded in the jacket of the second ASTRA conductor ('Hx').

to the helium flow cross-section ~93 mm^2. In the case of the ASTRA conductors, the rectangular cooling channel provides ~15 mm^2 section. The mass flow-rate of helium can be varied from ~1 to 10 g/s at the pressure of 10 bar. Given the SULTAN samples are tested in a vacuum environment, each conductor can be quenched individually, while avoiding a temperature rise in the neighbouring conductor. Further details on the cooling circuit are given in [37].

The three types of the SQD wires, which were found relevant for the following demonstration according to [40], are integrated in the grooves of the BISCCO and ASTRA conductors: MgB_2 monofilament wire in a stainless matrix of 0.3 mm diameter, MgB_2 60-filament wire in a Cu-Ni matrix and Nb_3Sn bronze-route wires of 0.8 mm diameter etched before the heat-treatment. The performance of the wires in terms of their critical temperature as a function of external magnetic field and the off-state resistance was preliminary measured and reported in [40]. The 2 m-long wires are inserted in a fiberglass sleeve and glued in the grooves using STYCAST, see Figure 2. The epoxy glue and stainless jacket inhibit the thermal conduction to the SQD, thus decreasing the detection sensitivity compared to potential integration within the cable space. Nonetheless, it was chosen due to the simplicity of integration. As a relevant example, the co-wound voltage taps of ITER conductors are placed outside the steel jacket to simplify their integration, even though worsening their noise cancellation performance.

A bare optical fiber is also added in each groove. The F1 fiber was damaged during the first integration attempt upon removing a guiding scotch tape after epoxy curing because it was placed on top of the SQD wire and got stuck on the tape at the location of damage. Although the following fibers are placed beneath the SQD wires, the F2 fiber on the ASTRA conductor got also broken, presumably at the transition region between the narrow channel and wider terminal section of the groove. The two fibers installed successfully ('F3' and 'F4') are in the grooves with the Nb_3Sn SQD wires. Outside the groove, the fibers are protected by Teflon tubing. Each fiber is about 12 m long (including the 2 m-long section on the conductor itself), which is routed inside SULTAN with the ends plugged in a feedthrough flange.

All the SQD wires showed no issues after the integration, maintaining electrical insulation from the conductor, thus allowing their independent operation at a certain transport current. As discussed in the following section, the measured properties are also in agreement with the preliminary expectations based on the short sample measurements [40]. Thin insulated copper wires are soldered at the ends of the SQD wires, see the photographs in Figure 2. One can also see the cross-section of the ASTRA conductor jacket showing the SQD wires and optical fibers, which was obtained after the test in SULTAN. Similar photo for the BISCCO conductor is not available because the conductor was not disassembled after the testing.

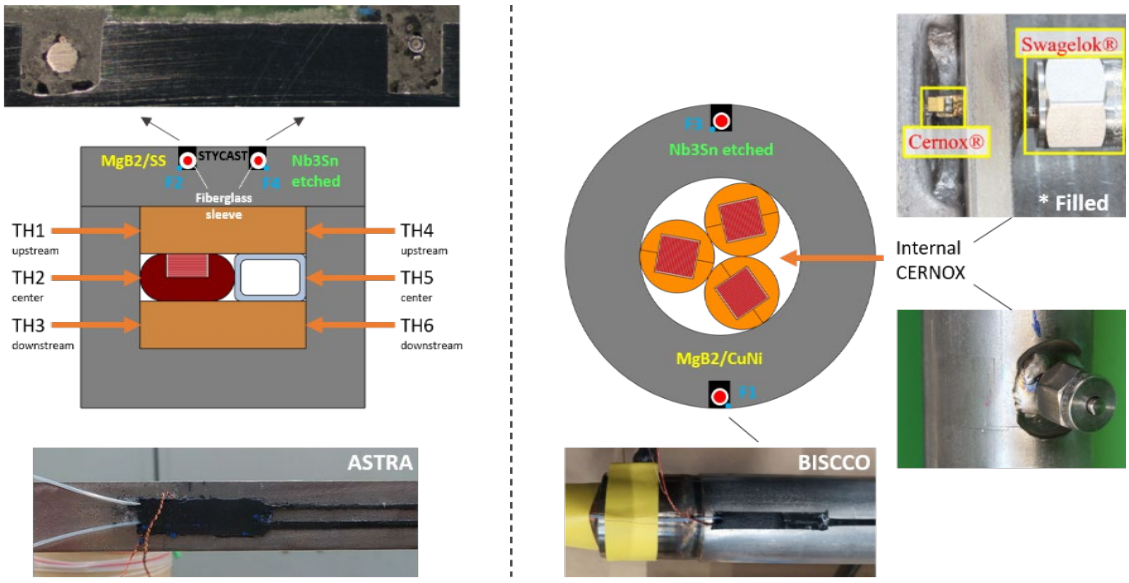

Figure 2. Cross-section of the ASTRA (left) and BISCCO (right) conductors including the SQD wires and optical fibers glued by STYCAST in the grooves on the steel jackets and photographs of the instrumentation. Note that the top photograph showing the cross-section of the grooves in the ASTRA jacket was obtained after the test in SULTAN. The top-right photograph of the Swagelok fitting is taken on the Filled conductor.

The 4-wire sensing method is used to measure resistance of the SQD wires over the full length and also the 20 cm section in the high-field zone.

The four cartridge heaters of about 3 mm diameter (1/8 inch), 25 mm length (1.0 inch) and ~20 Ω resistance are inserted in the steel jacket of the second ASTRA conductor. The two of them, 'H2' and 'H3', are near the center of the high-field zone, the other two, 'H1' and 'H4', – near the ends located at 200 mm distance from the center. In contrast to the conductor heating by increasing the temperature of inlet helium, they allow initiating a quench in a more localized manner.

3. Experimental results and numerical assessment

So far, there were five test campaigns focused on HTS 'quench experiments' carried out in SULTAN, with the corresponding test conditions outlined in Table 2. The first test on the sample made of the Ref conductor and an identical one made of non-soldered strands ended prematurely in the first quench run, when the latter conductor was burnt. This was caused by too late manual current switch off. As a result, an automatic sample protection system was implemented.

The two following tests on the HTS triplets allowed to study the quench dynamics initiated by warming up the inlet helium using heaters wound around helium pipes. The sample made of the Filled and No-twist conductors was repeatedly quenched at 6 T, 15 kA and 11 T, 11 kA operating conditions, progressively reaching higher and higher hot-spot temperatures. The same was done on the sample containing the Ref conductor (the one used in the first test) and BISCCO conductor at 4 T, 15 kA and 9 T, 10 kA.

The next test has been performed on the ASTRA and BISCCO conductors. Following the extensive DC and AC characterization of the conductors, the ASTRA leg was also burnt on the fourth quench run. This time the reason was a poor termination design, where a short region of the strand was not stabilized by the copper bars. Although it was considered as a design feature that would provide the possibility for a direct cooling (i.e. by preventing solder filling of the cable space during the termination soldering), the initial assumption that the ~1 cm-long section is short enough to be effectively cooled by conduction turned fatal. No quench tests were performed on the BISCCO conductor in this campaign.

Table 2. Overview on the performed quench measurements.

Test	SULTAN Sample	Quench conditions	Comments
QE1	L: Ref (not soldered) R: Ref	L: 7 T, 12 kA	Left leg burnt in the 1st quench run by overcurrent operation at 15 K
QE2	L: No-twist R: Filled	L & R: 6 T, 15 kA / 11 T, 11 kA	Inlet helium heating by pulsed and continuous operation. Gradual increase of Tmax to study its impact on the DC performance
QE3	L: BISCCO R: Ref	L & R: 4 T, 12 – 15 kA / 9 T, 9.5 kA	
QE4	L: BISCCO R: ASTRA	R: 11 T, 15 kA / 6 T, 15 kA	Right leg burnt in the 4th quench run by pulsed inlet helium heating
QE4 retest	L: BISCCO R: ASTRA2	L: 9 – 15 kA at 6 T, 9 T / 9 – 12 kA at 11 T R: 9 – 15 kA at 0 T, 6 T, 9 T, 11 T	Quenches by overcurrent and embedded heaters (ASTRA) and pulsed inlet helium heating (both)

By revising the termination design of the ASTRA sub-size conductor, it was re-built aiming only at the 'indirect' cooling (i.e. helium flows only in the tight cooling channel). The sample was finally tested in a wide range of the operating conditions (9-15 kA, 0-10.9 T) applying 'pulse' helium heating on both legs. In addition, quenches initiated by embedded heaters and overcurrent operation were also performed on the ASTRA leg.

The measured DC performance of the conductors at 10.9 T background magnetic field is compared in Figure 3. The critical current obtained at the 1 μV/cm criterion are within few percent from the expected values for the ASTRA conductor, about 5% lower for the BISCCO, Filled and No-twist and up to ~25% lower for the Ref and ASTRA2 conductors. The reasons of the reduction are being investigated, however not preventing the quench measurements, for which the variation of the performances is actually useful to obtain a broader view on the quench dynamics. Note a wide range of the n-values of the V-I transitions, from ~8 up to ~40. Its impact on the conductor thermal stability is further considered below.

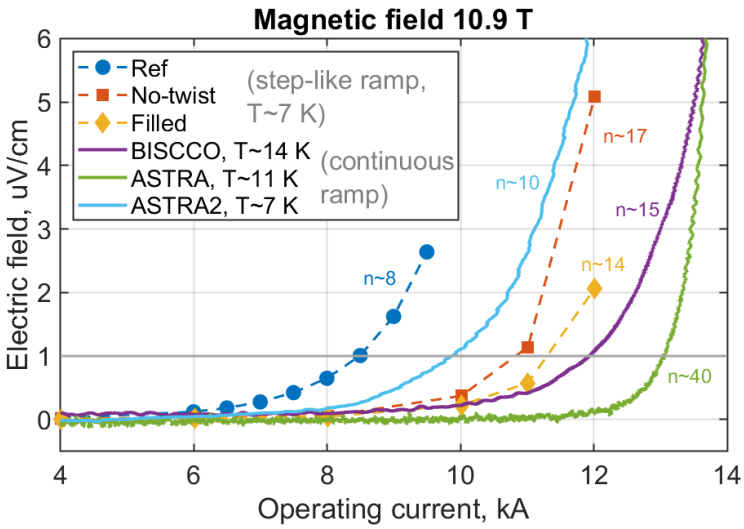

Figure 3. Voltage-current transitions of the conductors at 10.9 T background field and various operating temperatures using a step-like and continuous ramp of the transport current.

In order to interpret the observed behaviour of the conductors during the quench measurements, the following heat balance equation is considered:

$$CS\frac{\partial T}{\partial t} = I^2 R_1(I,T) + \frac{\partial}{\partial x}\left(kS\frac{\partial T}{\partial x}\right) - q_{He}P \text{ [W/m]}, \quad (1)$$

which applies to a certain cross-section S of the conductor with the uniform temperature distribution and accounts for the dependence on time t and longitudinal coordinate x. The contributions of copper, steel, superconductor and helium flow on the main thermo-electrical properties can be outlined as follows:

- The heat capacity term CS (in J/m/K) is a sum $(CS)_i$ for the involved materials. Considering their full amount, it is strongly dominated by steel (>70% contribution). Impact of helium becomes negligible above 10 K due to the strongly decreasing density with temperature.
- The electrical resistance per unit length $R_1(I,T) = \rho(I,T)/S$ (in Ω/m) as a function of the operating current I and temperature T for a given magnetic field has three distinctive modes: the one defined by superconductor for I and T near the superconductor critical surface, the current-sharing regime between superconductor and normal metals typically up to ~40 K and the normal-type operation at higher temperatures driven by copper. The current-sharing is assessed by solving an equality of the electric fields along the superconductor and normal metals, neglecting transverse currents. In this calculation, n-value is considered as a constant value in the range from 10 to 40. Impact of steel on the specific resistance of the conductors in the normal state is within 5%. The critical current density as a function of magnetic field and temperature, required to calculate the resistivity of superconductor, is taken according to the scaling laws reported in [1] for ReBCO and [43] for BISCCO tapes.
- The thermal conductivity term kS (in W.m/K), a sum of $(kS)_i$, is dominated by copper. Note that the material properties (C, ρ, k) as a function of temperature (and also magnetic field in case of ρ and k of copper) are evaluated based on the Cryosoft material database [44].
- The cooling term $q_{He}P$ (in W/m) features the wetted conductor perimeter $P = \pi D_h$ and the cooling flux of the forced flow helium q_{He}, which can be expressed as $q_{He} = Nu \cdot k_{He}\,(T - T_{He})/D_h$ for the Nusselt number $Nu = 0.026Re^{0.8}Pr^{0.4}(T_{He}/T)^{0.716}$ [45], the Reynolds number $Re = 4\dot{m}/\pi D_h \mu$ and the Prandtl number $Pr = \mu c_{He}/k$. The hydraulic diameter D_h is order of few mm for the test conductors and the mass flow-rate $\dot{m}$ is a free parameter set in the experiment in the range from 1 to 10 g/s. This assessment requires the use of the helium thermal conductivity k_{He}, viscocity μ and heat capacity c_{He} as a function of its pressure p and temperature T_{He}, which can be found tabulated in [46]. A certain value of T_{He} will be assumed in order to avoid the complete hydraulic analysis of the turbulent helium flow. Note a strong impact of $\dot{m}$ on the cooling power, increasing it from ~40 W/m at 1 g/s up to ~200 W/m at 10 g/s for $p = 10$ bar, $T_{He} = 5$ K and $T = 10$ K.

3.1. Stability

Although the stability study was not among the main objectives of the quench experiments, the deposited energy is often increased gradually in the measurements until a thermal runaway is finally observed on the conductors. This allows to identify the critical operating parameters, such as temperature and electric field, for a stable operation at the given operating current, magnetic field and helium flow.

For example, a comparison of the observed performance on the No-twist conductor operated at 15 kA, 6 T and 1.5 g/s flow is presented in Figure 4 for the two heating pulses. The first pulse is about 14 s long at 86 W heating power, thus releasing in total 1.2 kJ energy. Once heated helium reaches the conductor volume, increase of the temperatures and voltages and decrease of the mass flow-rate is observed. However, the conductor recovers from the disturbance, reaching the maximum temperature of about 16 K and 1.9 mV voltage. Corresponding voltage contributions from the four 10 cm long sections increase downstream the conductor as 13%, 21%, 30% and 36%. In contrast, applying the heat pulse during 16 s, the initial temperature and voltage response is nearly identical, but it leads eventually to the conductor quenching. The operating current is then switched off when the peak temperature increases up to 100 K, almost after 70 s since the beginning of the pulse.

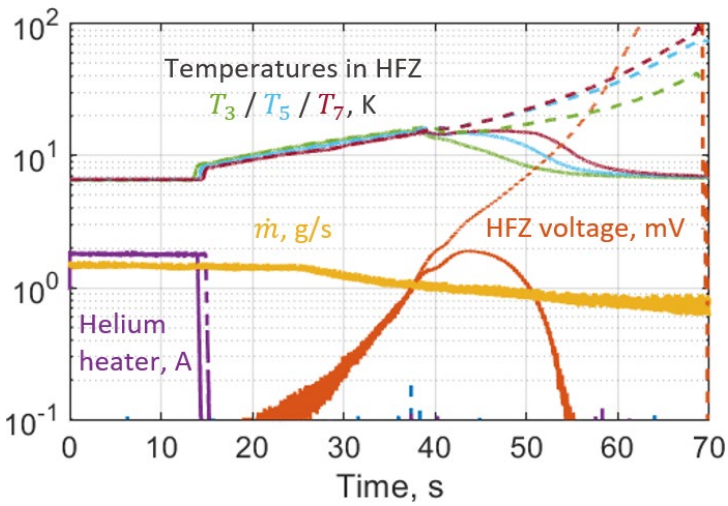

Figure 4. Evolution of temperatures, voltages and helium mass flow-rates for the two heating pulses applied on the inlet helium of the No-twist conductor operated at 6 T, 15 kA. Solid lines correspond to the slightly shorter pulse leading eventually to the conductor recovery, dashed lines – quench by the longer pulse.

Similar values of the quench voltage, though less accurate, are observed on the other triplet conductors. The filled conductor recovers after reaching ~3 mV, but quenches once ~4 mV is developed. These two values are ~2 mV and ~3 mV for the Ref conductor, whereas ~0.5 mV and ~0.6 mV for the BISCCO conductor.

The recovery behaviour is analysed in terms of the 'cold-end' recovery, also known as the 'equal-area' theorem [47]. This method provides solution for the equation (1) in the case of stationary operation (i.e. $\partial T/\partial t = 0$), which can be expressed as follows:

$$\int_{T_0}^{T_q} (I^2 R_1(I,T) - q_{He}P) \cdot k \cdot dT = 0, \tag{2}$$

where T_0 and T_q are the initial and quench temperatures. The equation terms are presented as a function of temperature for the ReBCO triplet conductors operated at 15 kA, 6 T and 1 g/s cooling in Figure 5.

The two assumptions are considered in the calculation for the helium temperature: $T_{He} = 5$ K independent of the conductor temperature (dashed line) and imposing a 5 K limit on the difference

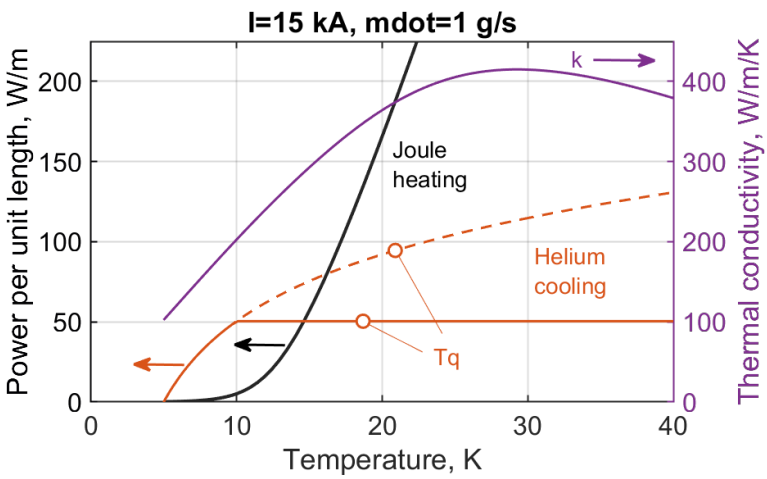

Figure 5. Assessment of the Joule heating, helium cooling and thermal conductivity as a function of temperature for the ReBCO triplets.

between them (solid line). Under these assumptions, the T_q solutions of the equation (2) are respectively 20.9 K and 18.7 K, see the circles in Figure 5. At these points, the Joule heating is about 2 to 3 times higher than the cooling power.

The minimum propagating zone (MPZ) can be estimated from the equation (1) assuming that $\partial T/\partial t = 0$, simplifying the heat conduction term as $kS(T_q - T_0)/MPZ^2$ and also accounting for the cooling term, thus $MPZ = \sqrt{kS(T_q - T_0)/(I^2R_1 - q_{He}P)}$. It yields $MPZ \approx 15$ cm for the case considered above and the quench voltage $V_q = MPZ \cdot IR_1(I, T_q) = 1.8$ mV. Note relatively low value of adiabatic quench energy (i.e. the enthalpy difference for the operation at T_0 and T_q of the conductor section of the MPZ length), which is only about 30 J compared to the energy required to trigger the quench (~kJ). This highlights that the impact of cooling on the conductor stability is decisive.

The quench temperature is also obtained on the second ASTRA conductor. It decreases from about 35 K at 9 T to 29 K at 10.9 T for the operation at 9 kA, 1 g/s and from 24 K at 9 T to 22 K at 10.9 T for the operation at 12 kA, 2 g/s. The results are shown in Figure 6 as a function of the operating current together with the predicted curves based on the 'cold-end' recovery method for the operation at 10.9 T and various cooling rates.

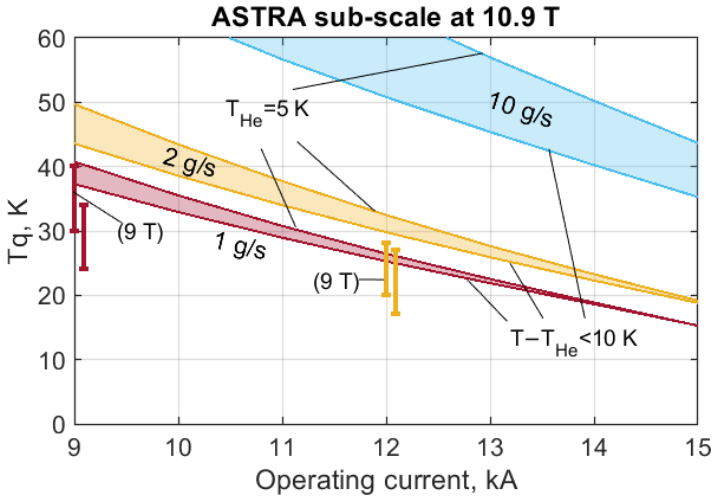

Figure 6. Quench temperature of the ASTRA conductor at various operating currents, magnetic fields and helium mass flow-rates.

The n-value, which characterises steepness of the voltage-current transition, is set at 15 in the calculation. It corresponds to that obtained on the second ASTRA conductor, although much higher value, about 45, was observed on the first one (see Figure 3). Note that the n-value has a strong impact on T_q, decreasing it from ~24 K at n=10 down to ~10 K at n=45 for the operation at 15 kA, 11 T, 2 g/s.

The calculated MPZ and quench voltage are similar to those obtained on the triplet conductors, falling in the range of 10 to 20 cm and 1 to 10 mV, depending on the operating conditions. The measured quench voltage is in the same range, except the two measurements performed at 9 kA and using the two heaters H2 and H3, resulting in the voltage recovery after reaching 11.2 mV at 9 T and 12.5 mV at 6 T.

Considering the specific resistance of the ASTRA conductor, the quenching conditions are reached in the range of 1 to 10 μΩ/m, near the end of the current sharing operating mode. This can be seen in Figure 7, where the performance of the conductor in that range becomes nearly identical to the one corresponding only to copper and steel, excluding the superconductor. The beginning of the current sharing mode, which can be defined at the voltage threshold of 1 μV/cm, is also indicated by the current sharing temperature T_{cs}, which corresponds to the specific resistance order of 10^{-2} μΩ/m, i.e. 2 to 3 orders of magnitude lower than the range where the quenching conditions can be reached.

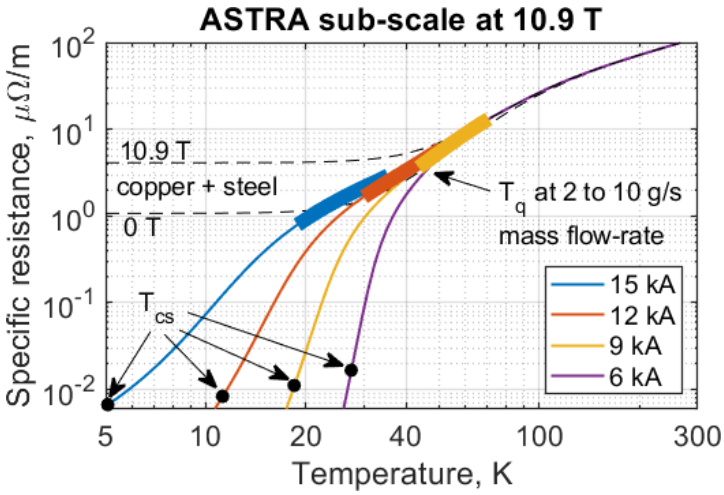

Figure 7. Specific resistance of the ASTRA conductor as a function of temperature at 10.9 T and various operating currents. The current-sharing temperature and quench temperature are also marked on the curves.

3.2. Quench propagation

Once the conductors are actually quenched, the operating current is kept constant until their thermal runaways reach certain limits in terms of the measured voltage or peak temperature. After that, the operating current is switched off almost instantaneously and they start recovering to the nominal operating conditions.

An example of the electric field evolution along the BISCCO and ASTRA conductors is shown in Figure 8. For the BISCCO conductor operated at 12 kA and 10.9 T, quench initiates at the beginning of the high-field zone (HFZ) of about 0.4 m length caused by the 30 s heating pulse at 160 W applied on the helium inlet flow, see the left plot. Relatively fast and uniform propagation over the entire HFZ and also partially outside of it is observed. In contrast, quenching the ASTRA conductor at 12 kA, 10.9 T by 10 s pulse at 170 W on the helium flow (the central plot), the runaway starts at the end of HFZ and then propagates slower mostly in the downstream direction of the helium flow. The right plot corresponds to the overcurrent operation of the ASTRA conductor at 15 kA, 10.9 T, leading to the quench initiation at the start of HFZ, but then quickly propagating downstream over the entire HFZ.

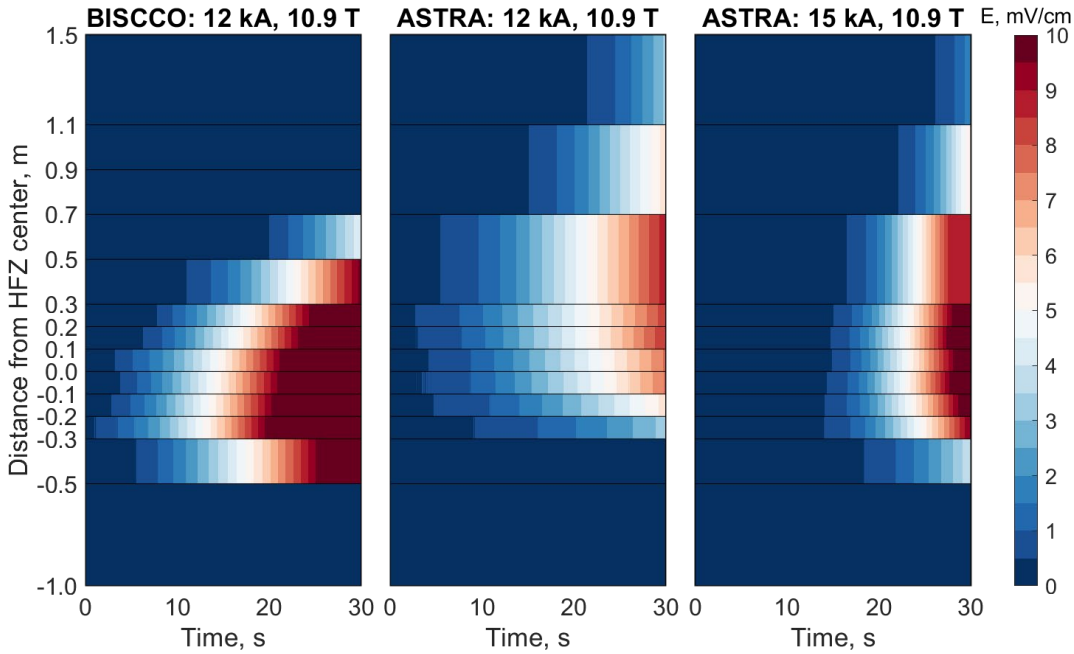

Figure 8. Evolution of the electric field along the BISCCO and ASTRA conductors during the last 30 seconds before the current switch-off.

Using the embedded heaters on the second ASTRA conductor, the quench dynamics is presented in Figure 9 for the operation at 9 kA and 6 T. All the three studied cases, using Heater 1 at the beginning of HFZ (-0.2 m wrt to the HFZ center), Heater 2 and 3 near the center (-0.01 m and 0.01 m) and Heater 4 at the end (0.2 m), results in rather localized resistive zone centred at the actual quench trigger. The duration of the heating pulses is about 50 s at 75 W power per each heater.

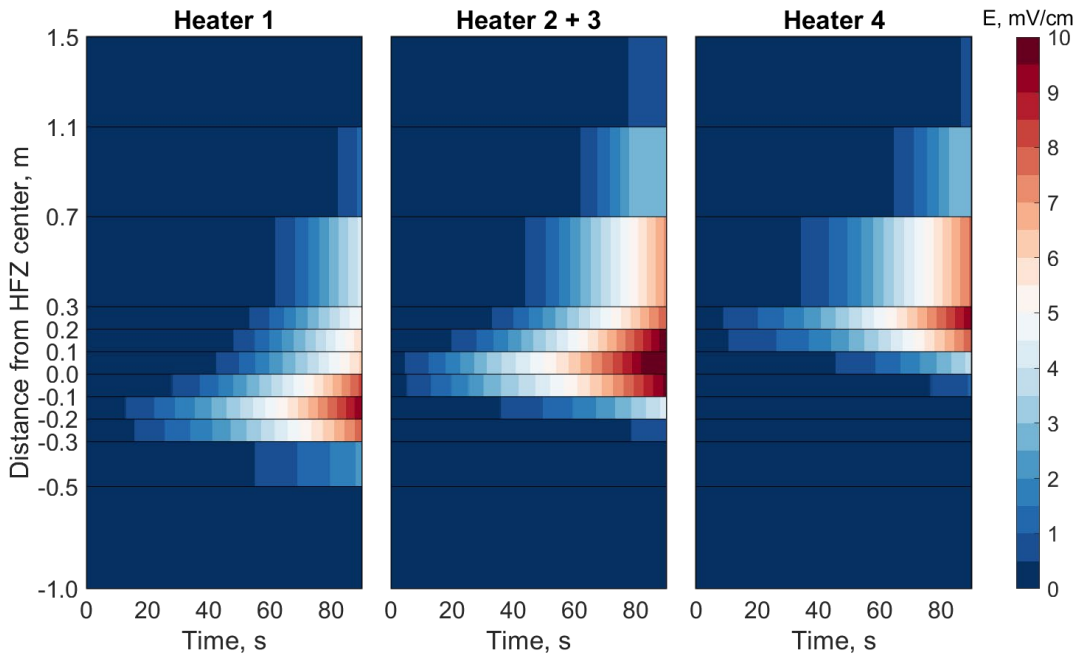

Figure 9. Evolution of the electric field along the ASTRA conductor during the last 90 seconds before the current switch-off using the cartridge heaters embedded in the steel jacket at various locations as a quench trigger.

The maximum electric field in the performed measurements is typically around 10 mV/cm. Considering the specific resistance of the ASTRA conductor as a function of temperature (see Figure 7), the peak temperature can be estimated at about 200 K (~70 μΩ/m) and up to 300 K (~110 μΩ/m) for the operation at 15 kA and 9 kA, respectively. The temperature measured along the conductor follows the electric field distribution, although lower values are typically observed on the sensors compared to the estimate from the electric field, with the difference up to 50 K in some cases. However, some of the measured temperatures are actually higher than the estimated ones. Hence, it should be noted that a direct comparison is not justified because the estimate is based on the voltage obtained from a relatively long section (at least 10 cm long) and the temperature can vary significantly along such length.

An illustration of the electric field and temperature distributions is provided in Figure 10 for the triplet conductors at the moment of reaching 0.5 V total voltage, except the Filled conductor where this voltage was not achieved thus 0.4 V is set instead. The temperature estimates (dashed lines) are obtained from the electric field, similar to that discussed for the ASTRA conductor above, and shown only above 40 K, i.e. in the range where the impact of HTS on the electric field can be neglected. The measured temperatures (solid lines) are those from the sensors located in helium flow. They typically show higher temperatures

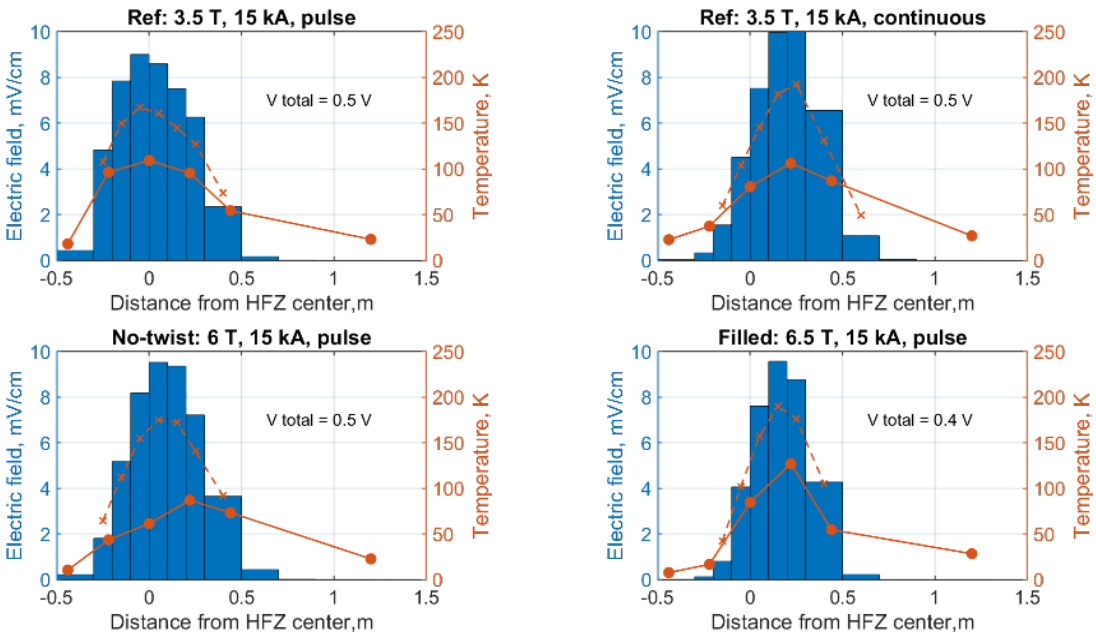

Figure 10. Distribution of the electric field (bars) and temperature (lines) for a given total voltage along the triplet conductors. Solid lines show measured data, dashed lines – estimated from the electric field.

compared to the sensors on the steel jacket, especially at the location of hot-spot. The difference is relatively low for the Filled and ASTRA conductors, deviating up to ~10 K and ~30 K, respectively. However, it increases up to ~50 K for the Ref and No-twist conductors, and even ~90 K for the BISCCO conductor.

Comparing the pulse and continuous heating applied on the Ref conductor, a downstream shift of the voltage and temperature profiles can be noticed. Although the measured peak temperature is around 100 K in both cases, the voltage profile is sharper and narrower in the latter case, with the peak slightly outside the high-field zone, at ~0.25 m coordinate. It is related to relatively weak dependence of the ReBCO critical current on magnetic fields, thereby the high-field zone defined as the 4 % SULTAN field homogeneity does not provide a strong confinement on the quench propagation.

Similar profiles are obtained on the No-twist and Filled conductors for the pulse heating. Larger discrepancy between the measured and estimated temperatures is observed on the triplet conductors, up to about 100 K for the Ref and No-twist conductors, and 55 K for the Filled one. It corresponds to the

enhanced thermal coupling between the steel jacket and cable in the Filled conductor. Its overall impact on the quench performance is further discussed in the next section, accounting also for the additional relevant observations reported below.

The BISCCO conductor, which should be identical to the Ref conductor in terms of the thermal coupling, demonstrates the temperature mismatch up to 70 K between the estimated and measured values. However, it varies among the quench runs performed at the same operating conditions (4 T, 15 kA, 1.5 g/s), with the maximum difference decreased down to 30 K for some of them.

Location of the maximum electric field and temperature does not change during the thermal runaway in the most of the performed measurements on all the conductors. As an example of the few exceptions observed, see again the voltage evolution in the overcurrent operation of the ASTRA conductor (the right plot in Figure 8).

Given the relatively high temperature range at which the conductors actually quench (~20 – 40 K), the time evolution of the maximum temperature T_{max} can be assessed by neglecting the heat conduction and cooling terms in the equation (1) and noting that the specific resistance R_1 becomes independent of the operating current (see Figure 7). As a result, T_{max} can be calculated from the following equation:

$$\int_{T_q}^{T_{max}} CS/R_1 \, dT = \int_0^t I^2 dt = q \,, \tag{3}$$

where the quench temperature T_q is used as the initial temperature and q is commonly referred to as the quench integral. T_q is set at 40 K in the following discussion. In order to justify the considered assumptions, impact of the current-sharing mode on the $T_{max}(q)$ dependence is studied in Figure 11. Note that time is set to zero at T=40 K, therefore q<0 at lower temperatures.

The curves obtained from the equation (3) (see the dashed lines) are compared to those from the equation (1), by neglecting the last two terms and considering T_{cs} as the initial temperature, thus $R_1(I,T)$ depending also on the operating current. As expected, the impact of the current-sharing is negligible for the temperatures above 40 K (i.e. q>0), thus superconductor can be neglected in that range of temperatures in the electrical and thermal considerations. At lower temperatures (i.e. q<0), the performance is determined by superconductor through the current-sharing term represented by $R_1(I,T)$, resulting in a strongly non-linear behaviour. The value of the quench integral required to increase the conductor temperature from Tcs up to 40 K decreases with the operating current despite the lower values of Tcs (i.e. higher margin to 40 K), from about 10^{10} A^2.s at 6 kA (~13 K margin) down to $0.5x10^{10}$ A^2.s at 15 kA (~35 K margin).

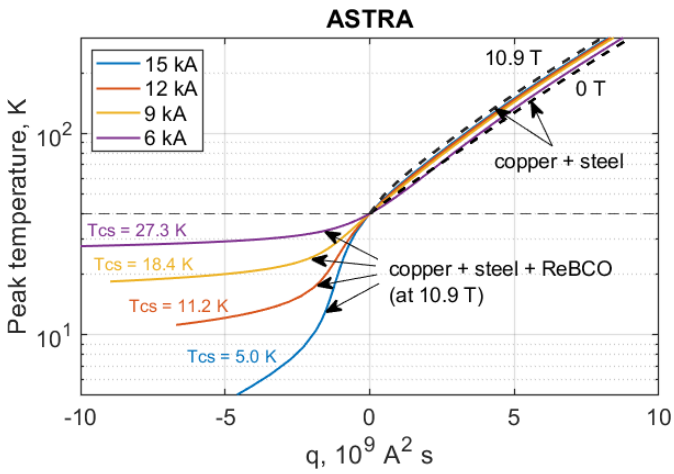

Figure 11. Peak temperature as a function of the quench integral for the ASTRA conductor using adiabatic assumptions.

The obtained curves are essentially linear in a semi-logarithmic scale for $T_{max} > T_q$. This allows to parametrize them as follows:

$$T_{max} = T_q e^{q/p}, \tag{4}$$

where the parameter p is a characteristic value of the quench integral q, which leads to $T_{max} = 2.71 T_q \approx 110$ K. By extracting q from the equation (4) and combining it with the equation (3), the following explicit expression can be derived for arbitrary temperatures T_1 and T_2: $p \approx \left(\int_{T_1}^{T_2} CS/R_1 \, dT\right)/(\ln T_2/T_1)$. It is proportional to CS, meaning a strong impact by the steel jacket as outlined in the beginning of the section. The actual values are extracted implicitly by fitting the $T_{max}(q)$ curves for the considered conductors based on their material composition (see Table 1). It was verified that p depends indeed linearly on the steel cross-section as suggested by the explicit expression. As a result, it can be expressed as $p = p_0 + f \cdot (p_1 - p_0)$, where p_0 and p_1 are the values calculated for the full and null cross-section of steel and the factor f is its relative fraction considered in the calculation. The values of p_0 and p_1 are reported in Table 3.

Table 3. The values of p considering zero (f=0) and full (f=1) cross-section of steel for the studied conductors.

Conductor	$\boldsymbol{p_0(f = 0)}$	$\boldsymbol{p_1(f = 1)}$
Ref, No-twist	1.14e9 A^2/s	7.18e9 A^2/s
Filled	2.10e9 A^2/s	8.02e9 A^2/s
BISCCO	0.73e9 A^2/s	5.62e9 A^2/s
ASTRA	1.28e9 A^2/s	4.43e9 A^2/s

The factor f provides a quantitative measure of the thermal coupling between the cable and steel jacket, expressing the 'perfect' coupling as $f = 1$ and the absence of it as $f = 0$. The actual values can be assessed from the measured $T_{max}(q)$ curves, which are summarized for the various operating conditions in Figure 12. The measured curves correspond to the highest temperature observed from the collection of the instrumented sensors.

Rather weak impact of the different operating currents, external magnetic fields and methods of the quench triggering (i.e. pulse and continuous helium heating, embedded heaters and overcurrent) is observed on the $T_{max}(q)$ curves, which confirms the validity of the considered adiabatic assumptions. A weak thermal coupling, expressed as $f \approx 0.25$, can be concluded for the Ref, No-twist and BISCCO conductors, which is due to localized contacts between the cable and steel domains. Improved effective heat capacity, corresponding to $f \approx 0.5$, is observed on the Filled conductor caused by a large contact area provided by solder. The highest effective heat capacity, $f \approx 0.6$, is for the ASTRA conductors following the large contact area and the pre-compressed conductor structure. However, note that the peak temperatures measured on the ASTRA conductors rise actually faster than those of the Filled conductor because the absolute cross-section of steel is ~50% lower.

The measured distributions of electric field are used to evaluate the quench propagation velocity (QPV) using a threshold of 1 mV/cm. It corresponds to the specific resistance of 5 to 10 μΩ/m and the estimated temperature of ~50 K (see Figure 7), thus ReBCO is still being in a superconducting state (critical temperature ~70 K at 11 T), although its current capacity becomes negligible compared to the large copper stabilizer, whereas BISCCO is already in the normal state (critical temperature ~30 K at 11 T). By obtaining the time moments of reaching the threshold among the distributed voltage taps, QPV can be estimated as ratio of the difference between the centers of the neighbouring sections and the difference between the corresponding moments. In that regard, QPV can be attributed to the location of each individual voltage tap, which can be considered virtually as a stopwatch point for the travelling resistive zone. However, the four locations cannot be used in this method, namely the two taps enclosing the first section, where the threshold was reached, due to uncertainty of the hot-spot initial location, and the two

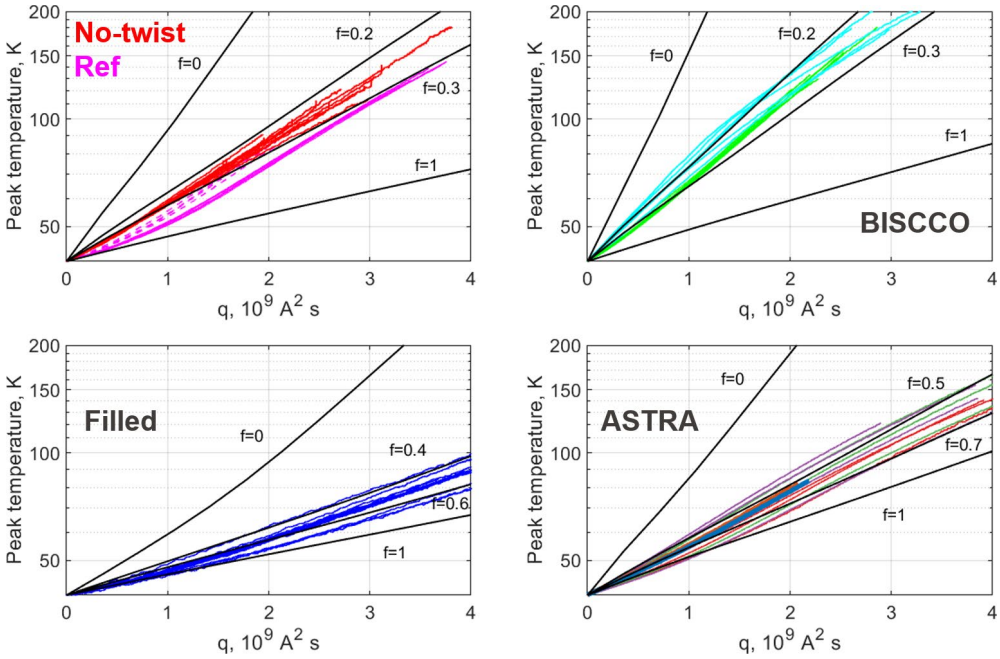

Figure 12. The peak temperature measured as a function of the quench integral and the calculated curves for various values of the factor f.

at the conductor ends. Focusing on the high-field zone containing 5 voltage taps spaced by 10 cm distance (Figure 1), at least three values of QPV can be evaluated.

QPV can also be assessed numerically. Accounting for the broad current-sharing mode in the conductors, the following expression is considered [48]:

$$QPV = \frac{I}{S}\left(\frac{\rho(T_t)k(T_t)}{C(T_t)\int_{T_0}^{T_t} CdT}\right)^{\frac{1}{2}} = I\left(\frac{R_1 \cdot kS}{CS\int_{T_0}^{T_t} CSdT}\right)^{\frac{1}{2}} \tag{5}$$

where T_0 is the initial operating temperature and T_t the transition temperature. The applicability of this formula for HTS is further justified in [49]. As T_t is defined for the propagating resistive zone, it is expected to be slightly higher than the quench temperature T_q, which corresponds to a stationary, non-propagating situation. Note that $QPV \sim 1/CS$, meaning that increasing the thermal coupling with steel ($f \to 1$) slows down the quench propagation, while the hot-spot build-up becomes also slower as the parameter p increases. The values of factor f obtained from the measurements (see Figure 12) are used in the following calculation.

The values of QPV obtained from the experiments and T_t that results in QPV of the same range, but derived from the equation (5), are summarized in Table 4. The data indicate at gradual increase of QPV and decrease of T_t by increasing the operating current. The values of QPV are typically in range from 10 to 100 mm/s, except those for the ASTRA conductors operated at 15 kA, which is due to very high n-value of the first conductor and the overcurrent operation of the second one, both leading to strong decrease of T_t down to ~10 K. The Ref and No-twist conductors demonstrate similar performance. Compared to the BISCCO conductor, they are of increased stability and slower quench propagation, whereas the opposite can be stated if compared to the Filled conductor. This corresponds to the lower critical temperature of the BISCCO tapes and the increased effective heat capacity of the Filled conductor by solder filling.

Table 4. Quench propagation velocity for various operating currents.

Conductor	I, kA	QPV, mm/s	T_t, K
ASTRA (f=0.60)	9	6 – 21	~35
	12	27 – 41	~30
	15	200 – 300*	~10
BISCCO (f=0.25)	12	30 – 100	~25
	15	40 – 90	~25
Ref (f=0.25)	12	13 – 20**	~40
	15	54 –66	~30
No-twist (f=0.25)	15	46 – 61	~30
Filled (f=0.50)	15	11 – 20**	~35

* obtained on ASTRA1 (n-value~40) and ASTRA2 overcurrent
** up-stream quench propagation

The total voltage developed along the conductor can be assessed in a simplified manner given that QPV is obtained for the conductor operation, at which impact of the superconductor becomes negligible on the electrical properties, i.e. corresponding to the operating temperature of ~50 K. As the specific resistance R_1 becomes a linear function of temperature (see Figure 7), integration of the electric field $E = I_{op}R_1$ along the length can be estimated as the peak electric field multiplied by the size of the resistive zone, i.e.

$$V \approx 2I_{op}R_1(T_{max}) \cdot QPV \cdot t \tag{6}$$

where T_{max} is the maximum temperature defined by the equation (4) and t denotes time, which is set at zero when $T_{max} = T_q$. Impact of the thermal coupling with steel on the total voltage is twofold, because T_{max} follows an exponential rise upon t/CS and the size of the resistive zone is proportional to t/CS. Therefore, increasing the thermal coupling would only lead to longer time to reach a certain value of the total voltage, but corresponding value of T_{max} at that voltage remains almost unchanged.

The measured data on the ASTRA conductor are compared to the results of the assessment using the values of QPV taken from Table 4 and the factor $f = 0.6$, see Figure 13. The calculation typically overestimates the measured voltage. This is clearly seen for the operation at 9 kA for the voltage above 0.2 V. This discrepancy should be primarily caused the quench propagation velocity, which is assumed constant in the assessment, whereas it decreases substantially in the SULTAN measurements once the propagating front exits the high-field zone of ~0.5 m length (see related discussion in [39]). Note that the measured voltage at the higher currents has an offset at zero time corresponding to the contribution from the resistive zone that reached the peak temperature of ~40 K, which is not included in the equation (6).

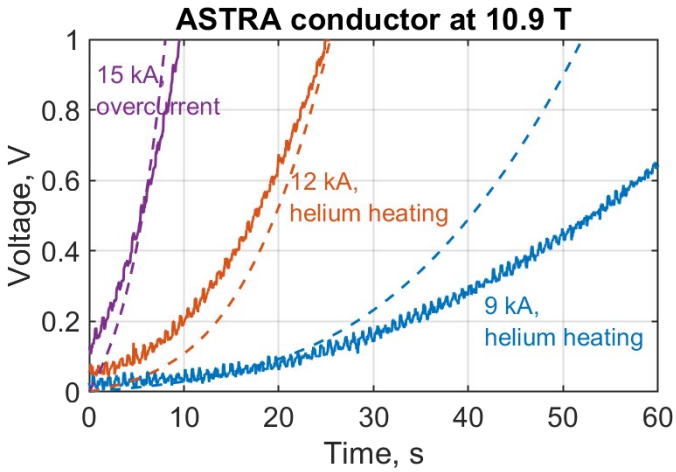

Figure 13. Total voltage along the ASTRA conductor during its quenching at various operating currents. Solid lines show the measured data, dashed lines – results of the calculation.

According to the equation (6), a linear dependence of the total voltage upon the maximum temperature is expected for the temperatures above 40 K. This correlation is also observed from the measurements, see Figure 14. The operating current has a strong impact on the measured curves, resulting in a counterintuitive trend of the maximum temperature decrease with increasing current for a given value of the total voltage. However, it can be understood from the terms comprising the equation (6), which actually indicates at the maximum temperature being inverse proportional to the quench integral, i.e. $T_{max} \sim V/(I^2 t)$. In contrast, impact of the magnetic field is relatively weak, affecting the maximum temperature of the BISCCO conductor within 10% deviation. Nonetheless, similar to the operating current, increasing the magnetic field reduces the maximum temperature at a certain voltage.

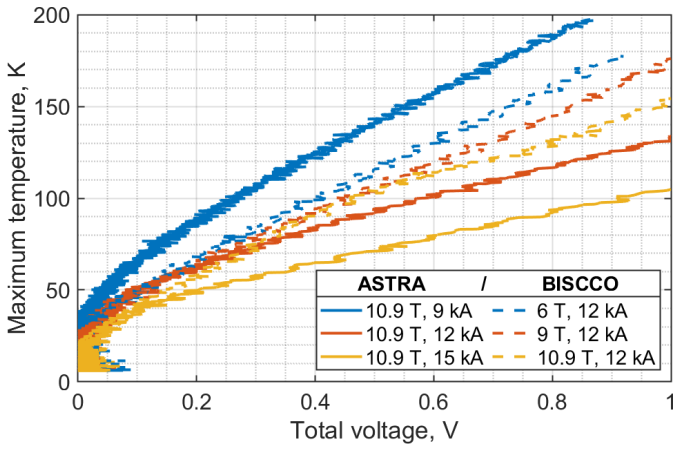

Figure 14. Maximum temperature on the ASTRA and BISCCO conductors as a function of the total voltage at various operating conditions.

3.3. Detection methods

Apart from the experience gained on the integration and operation of the optical fibers installed on the ASTRA and BISCCO conductors, no useful information concerning their actual detection performance is eventually obtained. Issues related to the detection sensitivity were actually expected due to negligible thermal contraction of fibers at temperatures below 50 K and also a high attenuation of the signal in the performed measurements, which is not yet fully understood. Considering the successful demonstration of the nearly identical optical method based on the optical fibers integrated in the cable space without a firm fixation, which is reported in [31], certain detection response was nonetheless expected. Unfortunately,

no evident correlation has been observed analysing the raw oscillating signal from the photodetector. For example, for those test runs where the minimum and maximum levels of the signal are maintained almost unchanged, counting the number of fringes per second is not correlated with the thermal runaway of the conductors. In multiple runs the levels are actually drifting, preventing a reliable data treatment. Decoupling the fibers mechanically from the test conductors might be suggested for future tests in order to obtain a reliable response.

The SQD wires were first characterized during the cool-down, warm-up and also during the DC measurements performed on the ASTRA and BISCCO conductors. The critical temperature (Tc) of the four wires as a function of the SULTAN DC background field (see Table 5) is in-line with the preliminary results obtained on the corresponding short wire samples, which are reported in [40]. Because of un-doped composition of the MgB_2 wires, their critical temperature decreases rapidly by the magnetic field. At 10.9 T it is even below the minimum operating temperature in the experiment of about 6.5 K, thus a proper operation is not possible at such conditions.

Table 5. Critical temperature of the SQD wires.

SQD wire	**Critical temperature Tc, K**			
	0 T	**6 T**	**9 T**	**10.9 T**
MgB_2/SS	~38	16.1	8.4	<6.5
Nb_3Sn etched R.	~18	14.8	13.3	12.5
MgB_2/CuNi	~38	20.5	10.5	<6.5
Nb_3Sn etched L.	~18	14.8	13.5	12.4

Resistance of the wires per unit length is measured from ~5 K up to ~300 K at zero magnetic field, see Figure 15. At the temperatures exceeding Tc by up to ~40 K, the normal state resistance is nearly constant at about 3.6 Ω/m for the MgB_2/SS wire and 0.07 Ω/m for the Nb_3Sn etched wires, whereas it increases

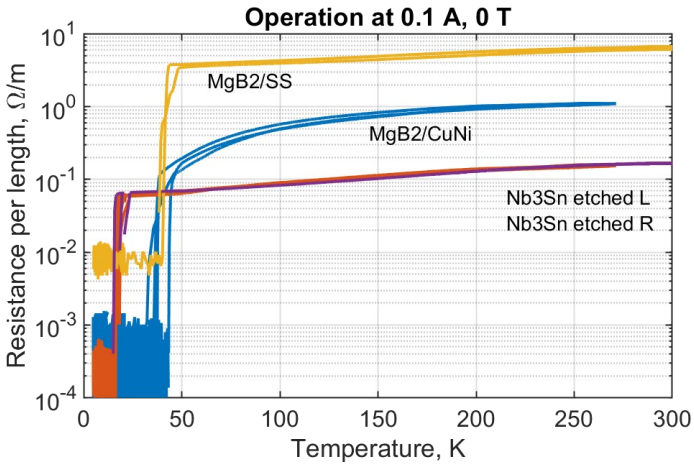

Figure 15. Specific resistance of the SQD wires as a function of temperature.

gradually for the MgB_2/CuNi wire up to 1.1 Ω/m at 270 K. The relatively low resistance of the Nb_3Sn wires could be compensated by increasing the operating current to achieve stronger absolute response, however it was kept fixed at 0.1 A in the experiment. Alternatively, thinner or even non-stabilized monofilament Nb_3Sn wires can also be used to increase the resistance. For example, up to 60 Ω/m is estimated for the external tin 0.13 mm wire used in the SULTAN conductor [50] and the wire size reduction down to 30 µm diameter is recently reported for the bronze route wires [51].

Given the weak dependence of the normal state resistance of the wires upon temperature, the measured resistance is normalized by the specific resistance near Tc. In case of relatively low peak temperature (up

to ~ Tc+40 K), such normalization corresponds to the length of the conductor resistive zone, which exceeds Tc of the wire. For example, the normalized signals are compared for the ASTRA conductor operated at 11 kA, 0 T, see Figure 16.

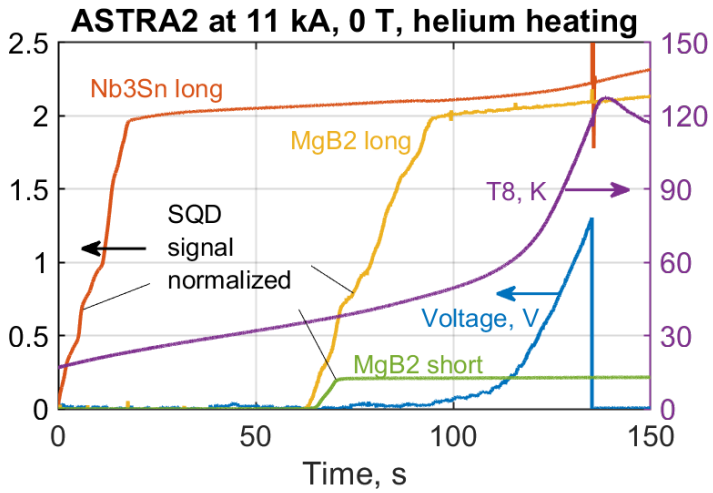

Figure 16. Response of the MgB_2/SS and Nb_3Sn etched SQD wires compared to the total voltage and peak temperature during the ASTRA conductor quench at 11 kA, 0 T.

At zero time, the peak temperature measured by T8 is about 17 K and the Nb_3Sn wire starts to react, reaching the 2 m equivalent length in 18 s, i.e. matching the actual total length of the instrumentation (see Figure 1). Afterwards, the increase rate sharply drops suggesting that the entire wire length is in the normal state. Similar reaction rate is observed on the MgB_2/SS wire, which starts at 36 K measured by T8 and takes around 7 s to saturate the 20 cm section in HFZ and 30 s to complete the transition over the 2 meters. The take-off temperatures obtained from T8 are nearly matching Tc of the wires, which allows concluding sufficient thermal coupling between the SQD wires and the conductor. One can estimate QPV as ~100 mm/s at ~20 K from the Nb_3Sn wire and ~29–67 mm/s at ~40 K from the MgB_2 wire. In contrast, the total voltage increases relatively slow during ~110 s, until the peak temperature reaches ~60 K, but starts to rise much faster afterwards. Note that one cannot attribute whether the SQD responce is still due to the quench trigger or already due to the quench propagation. However, this should not anyhow violate the idea of quench detection, i.e. detection of the exceeding temperature can never be a false positive event (assuming Tc(B) appropriately selected).

The in-field performances at 10.9 T of the Nb_3Sn SQD wire are shown in Figure 17 for the ASTRA conductor quenched by the helium heating and using the embedded heaters. The wire reaction starts at ~12 K measured by T8 and it saturates within ~15 s. The transition is slightly faster for the helium heating due to a more uniform distribution of the deposited energy. In both cases, acceleration of the transition can be seen after developing ~1 m long resistive zone.

The build-up of the SQD detection signal on the BISCCO conductor is more sophisticated, see Figure 18. The fast increase till ~1 m long resistive zone within 5 s, follows by a slower propagation during ~20 s at 9 T and ~30 s at 6 T till ~1.5 m length, after which it accelerates again. However, once the peak temperature increases above ~50 K, slightly before ~1.5 m length is reached, the used normalization of the SQD signal can no longer be interpreted simply in terms of the resistive zone length, because certain regions along the wire, which experience elevated temperatures, start increasing their specific contributions to the total signal.

Sufficient increase of the total voltage at least by 0.1 V is typically observed at the peak temperature of ~50–70 K. Regarding the SQD wires, increase of the resistive zone till ~1 m length, corresponding to the peak temperature of ~20–30 K, can be considered sufficient for triggering the quench protection. It results in the reduction of the quench detection time by 10–20 s.

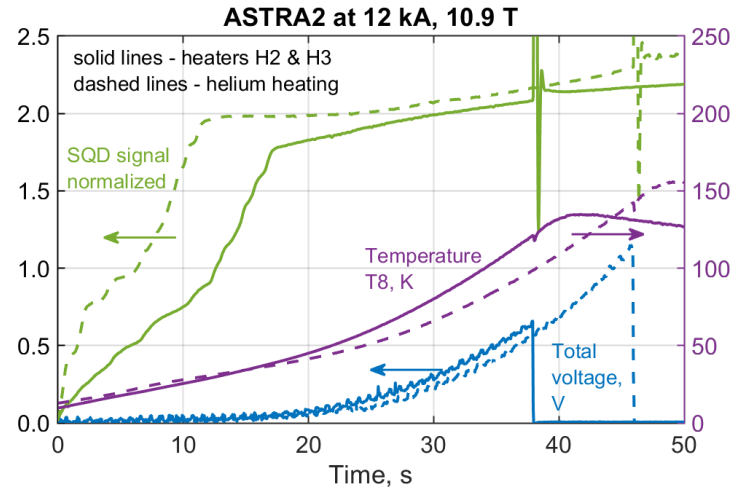

Figure 17. Response of the Nb_3Sn etched SQD wire on the ASTRA conductor at 12 kA, 10.9 T by using the embedded heaters (solid lines) and applying the helium heating (dashed lines)

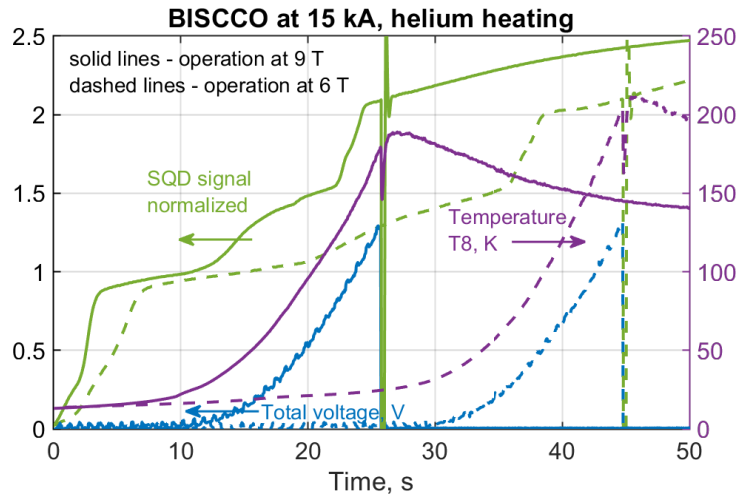

Figure 18. Response of the Nb_3Sn etched SQD wire on the BISCCO conductor at 15 kA, 9 T (solid lines) and 15 kA, 6 T (dashed lines).

4. Outlook on the coil windings

In contrast to the quench measurements in SULTAN, where the operating current is switched off instantaneously, the operating current follows an exponential decrease at certain time constant $\tau = L/R$ in coil windings with non-negligible inductance L, which are protected by external dump resistor R. The exponential discharge contributes to the quench integral as $\Delta q = \int_0^\infty \left(I_0 e^{-t/\tau}\right)^2 dt = I_0^2\tau/2$. In the large EU DEMO magnets, $\tau \approx 10$ s for the central solenoid modules and ≈ 30 s for the toroidal field coils. Due to relatively slow decrease of the operating current, additional increase of the hot-spot temperature is assessed below, considering for convenience the 15 kA Ref conductor discussed above. Even though the operating currents of the DEMO conductors are substantially higher than 15 kA, they also require proportionally larger cross-section of the components, thereby not changing essentially the outcome of the analysis.

Considering the total voltage developed along the conductor as the detection signal, the detection time t_0 is defined as $V(t_0) = V_{th}$, where V is calculated according to the equation (6) and V_{th} is the detection threshold. As a result, the hot-spot temperature is obtained as $T_{hot-spot} = T_{max}(I_0^2 t_0 + I_0^2\tau/2)$ using the

equation (4) and neglecting the quench validation time (typically ~1 s), which is applied to avoid false positives. The maximum temperature at the detection time, $T_{max}(I_0^2 t_0)$, is almost independent of the thermal coupling between the cable and steel represented by the factor f, as indicated previously in the discussion of equation (6). However, $T_{hot-spot}$ strongly decreases with increasing f because it only results in the increase of the conductor thermal capacity, see Figure 19.

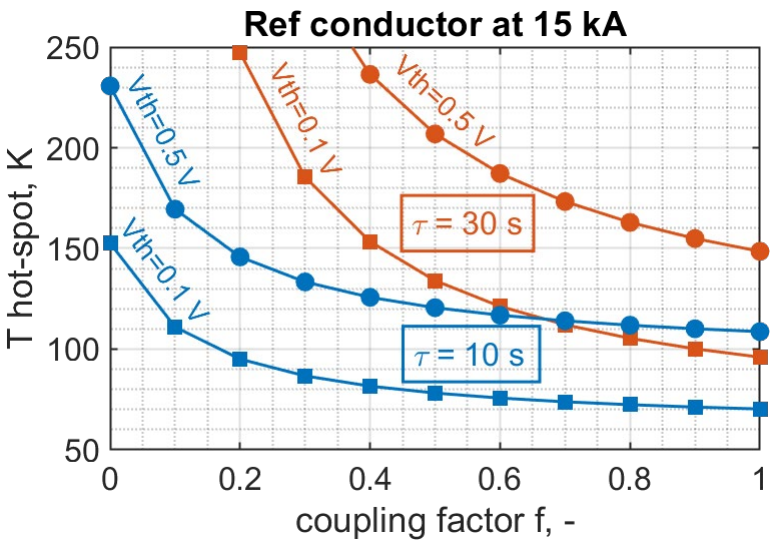

Figure 19. Assessment of the hot-spot temperature as a function of the thermal coupling factor in the triplet conductors for various discharge time constants and voltage detection thresholds.

The hot-spot temperature design criterion is typically set at 150 K on the steel jacket and ~250 K on the cable. In that regard, the conventional quench detection and protection systems applied at $\tau \approx 10$ s result in acceptable values of $T_{hot-spot}$, except for the very low values of f (<0.2) and high values of V_{th} (>0.1 V). At $\tau \approx 30$ s, the detection threshold of 0.1 V becomes unacceptable for the conductors with low the low thermal coupling, $f < 0.4$, whereas the entire range of f fails to fulfil the temperature requirement at 0.5 V detection. Note that the highest value of f observed so far in the measurements is ~0.7 (according to Figure 12). In that regard, decreasing the detection time or increasing the amount of stabilizer is required to avoid overheating. The first option is preferred as it does not affect the nominal magnet performance.

Considering the SQD wires to decrease the detection time, both Tc and the normal state resistance should be sufficiently high. Given that the voltage developed along the conductor at 0.1 V detection threshold is order of 0.1 V/m at the peak temperature of ~50 – 70 K, the normal state electric field of the wires of ~1 V/m should be pursued. This is a reasonable value considering thin wires (<0.5 mm diameter) at 0.1 – 1 A operating current. For the conductors having relatively low n-value of the voltage-current transition (~15), the quench temperature in the range from 30 K to 40 K would require to achieve the Tc in the same range to avoid potential false positives for the quench detection.

In that regard, proper operation of the SQD wires is not yet demonstrated in the quench experiments, as the MgB_2 wires, having sufficiently high off-state resistance, are of low Tc at high magnetic fields and the Nb_3Sn etched wires are of low off-state resistance, having Tc ~ 10 K at the high fields. The latter option, with the increased resistance by the wire size reduction, might still be applicable for the HTS conductors of the high n-value, which reduces substantially the quench temperature down to ~10 K (as observed on the first ASTRA conductor). Otherwise, achieving Tc of ~30 – 40 K at the high magnetic fields, up to 18 T for DEMO CS, is expected from MgB_2 doped wires or, more likely, iron based superconductors (see also [40]).

5. Conclusion

A series of sub-scale 15 kA 3.6 m-long conductors based on the stack of tapes soldered in copper profiles were measured in the SULTAN test facility at SPC aiming at the stability and quench characteristics. Those include the ReBCO and BISCCO triplet conductors as well as the sub-size ASTRA conductors, the single indirectly cooled strand operated in parallel field. The cross-sections of the material components used in the sub-scale samples are proportional to the designed full-size conductors such that the current densities are the same.

A very stable operation, featuring the quench temperature typically in the range from 30 K to 40 K is observed, which requires a large energy to initiate quench propagation. Lower values of Tq, down to ~10 K, are found on the conductors with the high n-value (~45) or when operated in the overcurrent mode due to presence of defects along the conductor length. The well-known 'equal area' stability method is also proven adequate to analyse the measured behaviour of the HTS conductors cooled by the forced flow of helium. The estimated and measured values of the quench voltage are in the range from 1 mV to 10 mV.

In the actual thermal runaways of the conductors, the developing voltage and temperature profiles basically follow an adiabatic release of the Joule heating, unlike the LTS conductors, whose performance is strongly affected by cooling effects during the quench propagation. Corresponding expressions for the peak temperature and total voltage are proposed and validated by the test results. As a result, enhancing the thermal coupling between the cable and steel jacket is found crucial to avoid overheating, despite the fact that it decreases the quench propagation velocity.

In order to address slow quench propagation, developing at the rate of ~10-100 mm/s in the experiment, the fast quench detection can be achieved by using the SQD wires, as demonstrated in the measurements using the MgB_2 and Nb_3Sn wires. Even though the SQD wires were integrated in the steel jacket of the ASTRA and BISCCO conductors, sufficient thermal coupling has been observed in the measurements. Depending on the actual quench temperature, optimal detection performance can be provided either by non-stabilized iron-based wires addressing the Tq range of 30 – 40 K at the high magnetic fields or Nb_3Sn thin wires for Tq ~10 K. The electrical field developed along the SQD wire in the normal zone has to be ~1 V/m to ensure superior performance of this detection method. The optimized performance and issues related to high voltage insulation at the extraction regions of the instrumentation is yet to be addressed. Even though the intended demonstration of the quench detection based on the optical interferometry did not succeed, further investigations of this method should be attempted.

HTS conductors for fusion with the high n-values (>30) may also be appealing in order to increase the propagation velocity because of the reduced stability. This is in contrast to fusion conductors made of LTS, for which decreasing the n-value is often proposed to enhance their stability.

Acknowledgment

The authors would like to thank Arooj Akbar and Bertrand Dutoit from EPFL for their interest and participation in the study of optical fibers for HTS fusion conductors, and Matt Rindfleisch from HyperTech Research, Inc. for the MgB_2 wires used in this work. The authors would also like to thank Paul Scherrer Institute for its technical support.

This work has been carried out within the framework of the EUROfusion Consortium, funded by the European Union via the Euratom Research and Training Programme (Grant Agreement No 101052200 — EUROfusion). Views and opinions expressed are however those of the author(s) only and do not necessarily reflect those of the European Union or the European Commission. Neither the European Union nor the European Commission can be held responsible for them.

References

[1] D. Uglietti, N. Bykovsky, K. Sedlak, B. Stepanov, R. Wesche, and P. Bruzzone, "Test of 60 kA coated conductor cable prototypes for fusion magnets," Superconductor Science and Technology, vol. 28, no. 12, p. 124005, Dec. 2015, doi: 10.1088/0953-2048/28/12/124005.

[2] Z. S. Hartwig et al., "VIPER: an industrially scalable high-current high-temperature superconductor cable," Supercond. Sci. Technol., vol. 33, no. 11, p. 11LT01, Nov. 2020, doi: 10.1088/1361-6668/abb8c0.

[3] M. J. Wolf, C. M. Bayer, W. H. Fietz, R. Heller, S. I. Schlachter, and K.-P. Weiss, "Toward a High-Current Conductor Made of HTS CrossConductor Strands," IEEE Transactions on Applied Superconductivity, vol. 26, no. 4, pp. 1–4, Jun. 2016, doi: 10.1109/TASC.2016.2525734.

[4] G. Celentano et al., "Design of an Industrially Feasible Twisted-Stack HTS Cable-in-Conduit Conductor for Fusion Application," IEEE Transactions on Applied Superconductivity, vol. 24, no. 3, pp. 1–5, Jun. 2014, doi: 10.1109/TASC.2013.2287910.

[5] T. Mito et al., "Development of FAIR conductor and HTS coil for fusion experimental device," J. Phys. Commun., vol. 4, no. 3, p. 035009, Mar. 2020, doi: 10.1088/2399-6528/ab7954.

[6] P. Mcintyre, J. Rogers, and A. Sattarov, "Blocks-in-Conduit: REBCO cable for a 20 T@20 K toroid for compact fusion tokamaks," IEEE Trans. Appl. Supercond., pp. 1–1, 2021, doi: 10.1109/TASC.2021.3064518.

[7] T. Mulder, D. van der Laan, J. D. Weiss, A. Dudarev, M. Dhallé, and H. H. J. ten Kate, "Design and Preparation of Two ReBCO-CORC Cable-In-Conduit Conductors for Fusion and Detector Magnets," IOP Conference Series: Materials Science and Engineering, vol. 279, p. 012033, Dec. 2017, doi: 10.1088/1757-899X/279/1/012033.

[8] V. E. Sytnikov, S. A. Lelekhov, A. V. Krasilnikov, V. V. Zubko, S. S. Fetisov, and V. S. Vysotsky, "Advanced Variants of HTSC Wires for TRT Electromagnetic System," Plasma Phys. Rep., vol. 47, no. 12, pp. 1204–1219, Dec. 2021, doi: 10.1134/S1063780X21110246.

[9] D. Uglietti, R. Kang, R. Wesche, and F. Grilli, "Non-twisted stacks of coated conductors for magnets: Analysis of inductance and AC losses," Cryogenics, vol. 110, p. 103118, Sep. 2020, doi: 10.1016/j.cryogenics.2020.103118.

[10] N. Yanagi et al., "Design and Development of High-Temperature Superconducting Magnet System with Joint-Winding for the Helical Fusion Reactor," Nuclear Fusion, vol. 55, no. 5, p. 053021, May 2015, doi: 10.1088/0029-5515/55/5/053021.

[11] N. Mitchell et al., "Superconductors for Fusion: a Roadmap," Supercond. Sci. Technol., Jun. 2021, doi: 10.1088/1361-6668/ac0992.

[12] R. Wesche et al., "Hybrid HTS-Nb3Sn-NbTi DEMO CS coil design optimized for maximum magnetic flux generation," Fusion Engineering and Design, Nov. 2018, doi: 10.1016/j.fusengdes.2018.10.027.

[13] V. Corato et al., "Strategy for Developing the EU-DEMO Magnet System in the Concept Design Phase," IEEE Trans. Appl. Supercond., pp. 1–1, 2022, doi: 10.1109/TASC.2022.3153248.

[14] N. N. Martovetsky and M. R. Chaplin, "Normal-zone detection in tokamak superconducting magnets with co-wound voltage sensors," IEEE Trans. Magn., vol. 32, no. 4, pp. 2434–2437, Jul. 1996, doi: 10.1109/20.511365.

[15] A. V. Dudarev et al., "Quench propagation and detection in the superconducting bus-bars of the ATLAS magnets," IEEE Transactions on Appiled Superconductivity, vol. 10, no. 1, pp. 381–384, Mar. 2000, doi: 10.1109/77.828253.

[16] S. Hasegawa, S. Ito, G. Nishijima, and H. Hashizume, "Fundamental Evaluations of Applicability of LTS Quench Detectors to REBCO Pancake Coil," IEEE Trans. Appl. Supercond., vol. 29, no. 5, pp. 1–5, Aug. 2019, doi: 10.1109/TASC.2019.2900633.

[17] J. Gao, B. Auchmann, C. Hug, A. Pautz, and S. Sanfilippo, "Study of a current-based quench detection method for CCT magnets via a co-wound superconducting sensing wire," IEEE Trans. Appl. Supercond., pp. 1–1, 2021, doi: 10.1109/TASC.2021.3059602.

[18] R. Kang, J. Wang, and Q. Xu, "Detecting Quench in HTS Magnets With LTS Wires—A Theoretical

and Numerical Analysis," IEEE Trans. Appl. Supercond., vol. 32, no. 6, pp. 1–5, Sep. 2022, doi: 10.1109/TASC.2022.3171185.

[19] M. Marchevsky, "Quench Detection and Protection for High-Temperature Superconductor Accelerator Magnets," Instruments, vol. 5, no. 3, p. 27, Aug. 2021, doi: 10.3390/instruments5030027.

[20] F. Scurti, J. D. Weiss, D. C. van der Laan, and J. Schwartz, "SMART conductor on round core (CORC) wire via integrated optical fibers," Supercond. Sci. Technol., vol. 34, no. 3, p. 035026, Mar. 2021, doi: 10.1088/1361-6668/abdc7f.

[21] E. E. Salazar et al., "Fiber optic quench detection for large-scale HTS magnets demonstrated on VIPER cable during high-fidelity testing at the SULTAN facility," Supercond. Sci. Technol., vol. 34, no. 3, p. 035027, Mar. 2021, doi: 10.1088/1361-6668/abdba8.

[22] Y. Liu, R. Mataira, R. Badcock, Z. Jiang, and J. Fang, "Application of Epoxy-Bonded FBG Temperature Sensors for High-Temperature Superconductor-Coated Conductor Quench Detection," IEEE Trans. Appl. Supercond., vol. 31, no. 2, pp. 1–8, Mar. 2021, doi: 10.1109/TASC.2020.3036368.

[23] J. D. Weiss, R. Teyber, M. Marchevsky, and D. C. van der Laan, "Quench detection using Hall sensors in high-temperature superconducting CORC-based cable-in-conduit-conductors for fusion applications," Supercond. Sci. Technol., vol. 33, no. 10, p. 105011, Oct. 2020, doi: 10.1088/1361-6668/abaec2.

[24] A. V. Dudarev, A. V. Gavrilin, Y. A. Ilyin, V. E. Keilin, and N. P. Kopeikin, "Superconducting windings with 'short-circuited' turns," Institute of Physics Conference Series, vol. 158, no. 2, pp. 1615–1618, 1997.

[25] S. Hahn, D. K. Park, J. Bascunan, and Y. Iwasa, "HTS Pancake Coils Without Turn-to-Turn Insulation," IEEE Trans. Appl. Supercond., vol. 21, no. 3, pp. 1592–1595, Jun. 2011, doi: 10.1109/TASC.2010.2093492.

[26] A. Anghel, "The quench experiment on long length cable-in-conduit conductor (QUELL) in SULTAN," J Fusion Energ, vol. 14, no. 1, pp. 129–139, Mar. 1995, doi: 10.1007/BF02214040.

[27] A. Anghel, "QUELL experiment: analysis and interpretation of the quench propagation results," Cryogenics, vol. 38, no. 5, pp. 459–466, May 1998, doi: 10.1016/S0011-2275(98)00016-2.

[28] C. A. Luongo, K. D. Partain, J. R. Miller, G. E. Miller, M. Heiberger, and A. Langhorn, "Quench initiation and propagation study (QUIPS) for the SMES-CICC," Cryogenics, vol. 34, pp. 611–614, Jan. 1994, doi: 10.1016/S0011-2275(05)80143-2.

[29] J. W. Lue and L. Dresner, "Normal Zone Propagation and Thermal Hydraulic Quenchback in a Cable-In-Conduit Superconductor," in Advances in Cryogenic Engineering, P. Kittel, Ed. Boston, MA: Springer US, 1994, pp. 437–444. doi: 10.1007/978-1-4615-2522-6_52.

[30] T. Ando, M. Nishi, T. Kato, J. Yoshida, N. Ito, and S. Shimamoto, "Propagation Velocity of the Normal Zone in a Cable-in-Conduit Conductor," in Advances in Cryogenic Engineering, R. W. Fast, Ed. Boston, MA: Springer US, 1990, pp. 701–708. doi: 10.1007/978-1-4613-0639-9_83.

[31] S. Pourrahimi et al., "Performance of the US quench detection systems in the QUELL experiments," IEEE Trans. Appl. Supercond., vol. 7, no. 2, pp. 447–450, Jun. 1997, doi: 10.1109/77.614530.

[32] K. Sedlak and P. Bruzzone, "Results and analysis of the hot-spot temperature experiment for a cable-in-conduit conductor with thick conduit," Cryogenics, vol. 72, pp. 9–13, Dec. 2015, doi: 10.1016/j.cryogenics.2015.07.003.

[33] A. Zappatore, W. H. Fietz, R. Heller, L. Savoldi, M. J. Wolf, and R. Zanino, "A critical assessment of thermal–hydraulic modeling of HTS twisted-stacked-tape cable conductors for fusion applications," Supercond. Sci. Technol., vol. 32, no. 8, p. 084004, Aug. 2019, doi: 10.1088/1361-6668/ab20a9.

[34] R. Heller, P. Blanchier, W. H. Fietz, and M. J. Wolf, "Quench Analysis of the HTS CrossConductor for a Toroidal Field Coil," IEEE Trans. Appl. Supercond., vol. 29, no. 7, pp. 1–11, Oct. 2019, doi: 10.1109/TASC.2019.2917154.

[35] R. Kang, D. Uglietti, R. Wesche, K. Sedlak, P. Bruzzone, and Y. Song, "Quench Simulation of REBCO Cable-in-Conduit Conductor With Twisted Stacked-Tape Cable," IEEE Trans. Appl. Supercond., vol. 30, no. 1, pp. 1–7, Jan. 2020, doi: 10.1109/TASC.2019.2926258.
[36] A. Zappatore, R. Bonifetto, R. Zanino, and X. Sarasola, "Effect of local defects on HTS fusion magnets performance," IEEE Trans. Appl. Supercond., pp. 1–1, 2022, doi: 10.1109/TASC.2022.3169718.
[37] O. Dicuonzo et al., "Upgrade and Commissioning of the SULTAN Facility to host Quench Experiments on HTS High Current Conductors," IEEE Trans. Appl. Supercond., vol. 31, no. 5, p. 9500505, Aug. 2021, doi: 10.1109/TASC.2021.3063997.
[38] O. Dicuonzo, "Electromechanical investigations and quench experiments on sub-size HTS cables for high field EU-DEMO Central Solenoid," PhD Thesis, EPFL, 2022. Available: http://infoscience.epfl.ch/record/293510
[39] A. Zappatore et al., "Quench experiments on sub-size HTS Cable-In-Conduit Conductors for fusion applications: data analysis and model validation," Submitted for publication in SUST, 2022.
[40] N. Bykovskiy, D. Uglietti, P. Bruzzone, and K. Sedlak, "Co-Wound Superconducting Wire for Quench Detection in Fusion Magnets," IEEE Trans. Appl. Supercond., vol. 32, no. 4, pp. 1–5, Jun. 2022, doi: 10.1109/TASC.2022.3140706.
[41] A. Akbar, Z. Yang, S. Wang, L. Thévenaz, and B. Dutoit, "Optical fibre sensing for fast hotspot detection in SFCLs," Supercond. Sci. Technol., vol. 33, no. 11, p. 115003, Nov. 2020, doi: 10.1088/1361-6668/abb200.
[42] N. Bykovsky, "HTS high current cable for fusion application," PhD Thesis, EPFL, 2017. Available: https://infoscience.epfl.ch/record/231964
[43] R. Wesche, "Temperature dependence of critical currents in superconducting Bi-2212/Ag wires," Physica C: Superconductivity, vol. 246, no. 1–2, pp. 186–194, May 1995, doi: 10.1016/0921-4534(95)80024-7.
[44] L. Bottura, "Solid Materials Database of CryoSoft." https://supermagnet.sourceforge.io/solids.html
[45] P. J. Giarratano, V. D. Arp, and R. V. Smith, "Forced convection heat transfer to supercritical helium," Cryogenics, vol. 11, no. 5, pp. 385–393, 1971.
[46] S. W. Van Sciver, Helium Cryogenics. New York, NY: Springer New York, 2012. Available: http://link.springer.com/10.1007/978-1-4419-9979-5
[47] B. J. Maddock, G. B. James, and W. T. Norris, "Superconductive composites: Heat transfer and steady state stabilization," Cryogenics, vol. 9, no. 4, pp. 261–273, Aug. 1969, doi: 10.1016/0011-2275(69)90232-X.
[48] R. G. Mints, A. A. Akhmetov, and A. Devred, "Enhanced quench propagation velocity," IEEE Trans. Appl. Supercond., vol. 3, no. 1, pp. 654–657, Mar. 1993, doi: 10.1109/77.233786.
[49] M. Bonura and C. Senatore, "An equation for the quench propagation velocity valid for high field magnet use of REBCO coated conductors," Applied Physics Letters, vol. 108, no. 24, p. 242602, Jun. 2016, doi: 10.1063/1.4954165.
[50] B. Jakob and G. Pasztor, "Fabrication of a high current Nb3Sn forced flow conductor for the 12 tesla SULTAN test facility," IEEE Trans. Magn., vol. 23, no. 2, pp. 914–917, Mar. 1987, doi: 10.1109/TMAG.1987.1064861.
[51] A. Kikuchi, Y. Iijima, M. Yamamoto, M. Kawano, and M. Otsubo, "The Bronze Processed Nb 3 Sn Ultra-Thin Superconducting Wires," IEEE Trans. Appl. Supercond., vol. 32, no. 4, pp. 1–4, Jun. 2022, doi: 10.1109/TASC.2022.3145286.